IOPscience

New Journal of Physics
The open access journal at the forefront of physics

Feasibility of quantum key distribution through a dense wavelength division multiplexing network

Bing Qi[1,2,4], Wen Zhu[2], Li Qian[1,2] and Hoi-Kwong Lo[1,2,3]

Published 27 October 2010 • IOP Publishing and Deutsche Physikalische Gesellschaft
New Journal of Physics, Volume 12, October 2010

+ Article information

Author e-mails

bqi@physics.utoronto.ca

Author affiliations

[1] Center for Quantum Information and Quantum Control, University of Toronto, Toronto, ON, Canada

[2] Department of Electrical and Computer Engineering, University of Toronto, Toronto, ON, Canada

[3] Department of Physics, University of Toronto, Toronto, ON, Canada

[4] Author to whom any correspondence should be addressed.

Dates

Received 7 June 2010

Published 27 October 2010

Citation

Bing Qi *et al* 2010 *New J. Phys.* **12** 103042

DOI

https://doi.org/10.1088/1367-2630/12/10/103042

Abstract

In this paper, we study the feasibility of conducting quantum key distribution (QKD) together with classical communication through the same optical fiber by employing dense-wavelength-division-multiplexing (DWDM) technology at telecom wavelength. The impact of classical channels on the quantum channel has been investigated for both QKD based on single-photon detection and QKD based on homodyne detection. Our studies show that the latter can tolerate a much higher level of contamination from classical channels than the former. This is because the local oscillator used in the homodyne

detector acts as a 'mode selector', which can suppress noise photons effectively. We have performed simulations based on both the decoy BB84 QKD protocol and the Gaussian-modulated coherent state (GMCS) QKD protocol. While the former cannot tolerate even one classical channel (with a power of 0 dBm), the latter can be multiplexed with 38 classical channels (0 dBm power per channel) and still has a secure distance around 10 km. A preliminary experiment has been conducted based on a 100 MHz bandwidth homodyne detector.

1. Introduction

One important practical application of quantum information is quantum key distribution (QKD), whose unconditional security is based on the fundamental laws of quantum mechanics [1, 2]. Today most of the fiber-based QKD experiments are conducted through dedicated 'dark' fibers. As the applications of QKD have been extended from point-to-point links to network configurations [3]–[5], it would be much more appealing if QKD can be conducted through the existing fiber network together with classical communication signals. In this 'coexistence' architecture, the quantum signal for QKD shares a common optical fiber with unrelated classical signals [6].

The coexistence architecture based on wavelength-division-multiplexing (WDM) technology was proposed by Townsend in the late 1990s [7] and has been studied thereafter [6], [8]–[11]. These studies show that the existence of strong classical traffic could be detrimental to the QKD channel. This is because a classical signal is typically many orders of magnitude stronger than the quantum

signal. Thus even a small crosstalk from a classical channel could overwhelm normal QKD operation. One feasible way is to place the quantum signal at the 1300 nm 'original' or O-band while placing the classical signal at the 1550 nm 'conventional' or C-band [6]. For such a large wavelength separation, both the leakage of the classical signal and the anti-Stokes Raman scattering can be effectively suppressed to a tolerable level.

However, in many cases there are advantages to placing both the quantum and the classical signals in the C-band. For example, fiber loss at the C-band is significantly lower than that at the O-band; hence the secure distance of QKD could be extended. Furthermore, this architecture is more compatible with today's fiber network.

In [10], a BB84 QKD system is multiplexed with classical signals using a C-band reconfigurable optical add drop multiplexer (ROADM). In [11], the authors multiplexed four classical channels with one quantum channel using C-band 100 GHz dense-wavelength-division-multiplexing (DWDM). This is a special case where four classical channels are used by legitimate users (Alice and Bob) for key distillation and encrypted communication. The total power of the four classical channels is only about −22 dBm. By placing the quantum signal at a non-adjacent channel of the classical signal, the maximum secure distance was shown to be around 40 km [11]. These previous studies suggest that with standard technology, it is still infeasible to place both the QKD signal and the strong classical signal (0 dBm) at the C-band.

We remark that all the previous studies have been conducted in QKD systems employing a single-photon detector (SPD), implementing, for instance, the standard BB84 QKD protocol. Here, we will show that QKD systems based on optical homodyne detection are inherently robust against noise due to multiplexing. Intuitively, this is because a

strong local oscillator (LO) is used to beat with the weak quantum signal during homodyne detection. Only photons in the same spatiotemporal and polarization mode as the LO can be detected while noise photons in different modes will be suppressed effectively. Thus the LO acts as a 'mode selector' [12]. We remark that in a recent free-space QKD experiment, an optical homodyne detector was employed to suppress ambient light [13].

In this paper, we study quantitatively the amount of noise photons added into the QKD channel in a typical DWDM setup. All the theoretical simulations were carried out based on the performance of commercial components. Two specific QKD protocols, namely, the decoy state BB84 protocol [14]–[16] and the Gaussian-modulated coherent state (GMCS) QKD protocol [17], were chosen for numerical simulations. The BB84 QKD protocol [1] is the first and the most well-known QKD protocol. Its unconditional security has been rigorously proved based on the laws of quantum mechanics [18], even when implemented on practical setups with some imperfections, such as weak coherent pulses, detector dark counts [19, 20] and detector efficiency mismatch [21]. The security of the GMCS QKD protocol was first proven against individual attacks with direct [22] or reverse [17, 23] reconciliation schemes. Security proofs were then given against general collective attacks [24]–[26]. To date, three groups have independently claimed that they have proved the unconditional security of GMCS QKD [27].

Our simulation results show that it is possible to multiplex GMCS QKD with a 0 dBm classical channel using a C-band 100 GHz DWDM without significantly reducing its performance. Even multiplexed with 38^{5} classical channels (0 dBm power each channel), GMCS QKD still has a secure distance around 10 km. A preliminary experiment was conducted based on a 100 MHz bandwidth homodyne detector.

We remark that although our studies are conducted in GMCS QKD, our conclusions should be applicable in other QKD protocols employing homodyne detection such as the discrete modulated continuous variable QKD protocol [28].

This paper is organized as follows. Section 2 contains the theoretical analysis of various noise sources in a generic quantum/classical signals coexistence scheme. In section 3, we quantify the contribution from each noise source based on the performance of commercial components. In section 4, we present simulation results in both the decoy state BB84 protocol and the GMCS QKD protocol. We also present preliminary experimental results with a 100 MHz shot-noise-limited homodyne detector. Section 5 is a brief conclusion.

2. Theoretical analysis on noise contribution

In a typical coexistence architecture based on DWDM, the noise photons in the quantum channel can be contributed by several sources [6, 10, 11], including the leakage photons from classical channels due to the finite isolation of DWDM components, the 'in-band' noise photons generated in optical fibers from nonlinear processes, such as four-wave mixing (FWM) and spontaneous Raman scattering, and the in-band amplified spontaneous emission (ASE) photons generated by optical amplifiers. Here, in-band noise refers to noise photons within the spectral bandwidth allocated to the quantum channel. In this section, we will quantify the amount of noise photons contributed by each of the above sources based on a typical DWDM configuration as shown in figure 1. In figure 1, we assume that an erbium-doped fiber amplifier (EDFA) is employed to boost the optical power of classical channels before multiplexing with quantum channels. Furthermore, we assume that all the classical channels are placed at wavelengths longer than that of the quantum channels, since the spontaneous anti-Stokes Raman scattering (SASRS) is

typically weaker than the spontaneous Stokes Raman scattering.

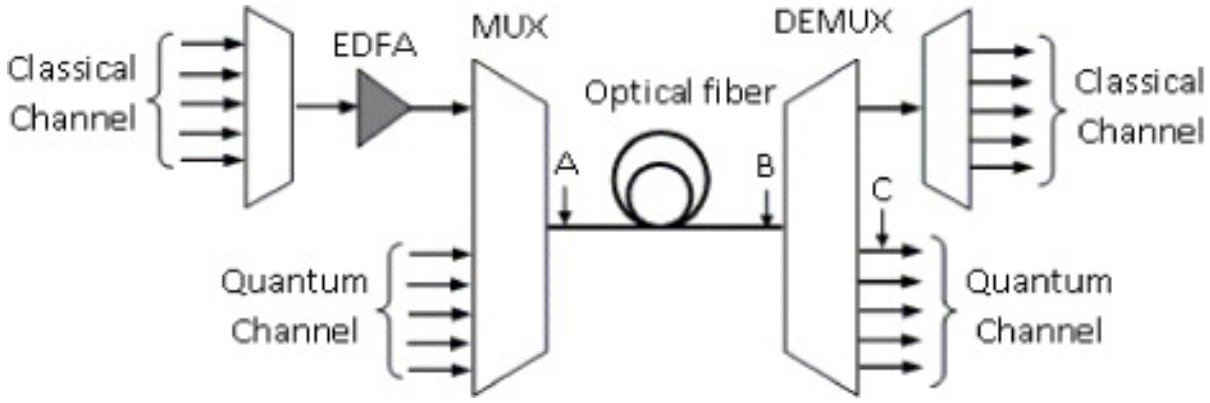

Zoom In Zoom Out

Reset image size

Figure 1. A typical scheme for multiplexing quantum channels with classical channels. MUX—multiplexer; DEMUX—demultiplexer; EDFA—erbium-doped fiber amplifier.

Download figure:

Standard Export PowerPoint slide

In this paper, we assume that the eavesdropper (Eve) can control all the classical channels and the EDFA (see figure 1) but she cannot access the multiplexer (MUX) and the demultiplexer (DEMUX) used for multiplexing the quantum signals with classical signals. One special example is that the classical signals are actually used by Alice and Bob for authentication, error correction and privacy amplification [11]. In the more general cases where classical channels are allocated to other users, Alice and Bob can place the MUX and DEMUX in their local secure stations. Under the above assumptions, the quantum signals sent by Alice are calibrated after MUX (point A in figure 1). Hence the performance of the QKD system is independent of the insertion loss of MUX. On Bob's side, the insertion loss of DEMUX

can be treated as part of the loss in Bob's detection system.

2.1. Amplified spontaneous emission (ASE) of an erbium-doped fiber amplifier (EDFA)

It is well known that an ideal, noise-free amplifier cannot exist [29]. In the case of an optical amplifier, the fundamental noise originates from the spontaneous emission. The ASE from a practical EDFA has a broad bandwidth of the order of tens of nm, which can be treated as a broadband noise source with a flat spectral power density within the spectral bandwidth of the quantum channel. We remark that a practical laser source also has a broadband noise background, which can be modeled as ASE from a virtual optical amplifier.

The average ASE photon number in one spatiotemporal mode is given by [30]

$$\langle N_{\mathrm{ASE}} \rangle = 2n_{\mathrm{sp}}(G-1). \tag{1}$$

Here factor 2 accounts for the two orthogonal polarization modes. G is the gain of the EDFA, and $n_{\mathrm{sp}} \geq 1$ is the spontaneous emission factor. If spontaneous emission is the only noise source (no excess noise), $n_{\mathrm{sp}}=1$.

In practice, the excess noise of an EDFA is commonly quantified by its noise figure (NF). In the unsaturated regime, NF is related to n_{sp} by [30]

$$\mathrm{NF} = \frac{1+2n_{\mathrm{sp}}(G-1)}{G}. \tag{2}$$

In the high-gain range ($G \gg 1$), $\mathrm{NF} \simeq 2n_{\mathrm{sp}}$.

Typically, the ASE power is much lower than that of the classical signal. However, its bandwidth is much broader and extends into the quantum channel. Thus, ASE will contribute to in-band noise. Fortunately, the MUX used at Alice's side functions as a bandpass filter and can greatly suppress this in-band ASE noise. Given that the cross-

channel isolation of MUX is ξ_1, the in-band ASE photon number (per spatiotemporal mode) measured at the output of MUX (point A in figure 1) is

$$\langle N_{\mathrm{ASE}}^{(A)} \rangle = 2\xi_1 n_{\mathrm{sp}}(G-1). \tag{3}$$

In this paper we will not consider the 'out-of-band' ASE noises, since they are typically much weaker than the classical signals themselves.

2.2. Leakage from the classical channel

Although the classical signal has a different wavelength from that of the quantum signal, a small fraction of the classical signal will leak into the quantum channel due to the finite isolation of DEMUX. In a BB84 QKD system, this leakage will contribute to out-of-band noise, which could be further reduced by using spectral filters at the receiver's end. In a GMCS QKD system, this leakage contributes noise photons in the 'unmatched mode' of the LO.

We define the power of the classical signal output from the communication fiber as P_{out} (measured at point B in figure 1). Given the isolation of the DEMUX ξ_2, the power of the leakage signal received by Bob (measured at point C in figure 1) is $P_{\mathrm{leak}}=\xi_2 P_{\mathrm{out}}$. The average leakage photon number per second is

$$\langle N_{\mathrm{leak}}^{(C)} \rangle = \frac{\xi_2 P_{\mathrm{out}}}{h\nu}. \tag{4}$$

Here h is Planck's constant and ν is the frequency of the classical signal.

2.3. Spontaneous anti-Stokes Raman scattering (SASRS)

As the strong classical signals propagate along the optical fiber, noise photons at different wavelength can be generated through various

nonlinear optical processes. If the wavelength of the noise photons coincides with that of the quantum signal, they cannot be filtered out at the receiver's end and will contribute to in-band noise. It has been shown that SASRS is the dominant nonlinear process when the quantum channel is placed at the shorter wavelength of the classical channel [6, 11].

The SASRS noise power within a bandwidth of ⊠⊠ (measured at point B in figure 1) is given by [6]

$$P_{\mathrm{SASRS}} = P_{\mathrm{in}}\beta z \eta_{\mathrm{ch}} \Delta\lambda = P_{\mathrm{out}}\beta z \Delta\lambda. \tag{5}$$

Here ⊠ is the spontaneous Raman scattering coefficient, P_{in} (measured at point A in figure 1) is the input power of the classical signal, z is the fiber length and η_{ch} is the transmittance of the optical fiber.

To estimate the noise photon number per spatiotemporal mode, we first use the relation ⊠=c/⊠ to determine the total mode number corresponding to a bandwidth of ⊠⊠ and a time window of ⊠t=1⊠s to be $N_{\mathrm{mode}} = |\Delta\nu\Delta t| = \frac{c}{\lambda^2}\Delta\lambda$. Here c is the speed of light in vacuum.

Given that the insertion loss of DEMUX is η_{DMU}, the in-band SASRS photon number (per spatiotemporal mode) measured at the output of DEMUX (point C in figure 1) can be calculated from (5):

$$\langle N_{\mathrm{SASRS}}^{(C)} \rangle = \frac{P_{\mathrm{SASRS}}}{h\nu N_{\mathrm{mode}}}\eta_{\mathrm{DMU}} = \frac{\lambda^3}{hc^2} P_{\mathrm{out}}\beta z \eta_{\mathrm{DMU}}. \tag{6}$$

Again, in the derivation of (6), we have used the relation ⊠=c/⊠.

2.4. Four-wave mixing (FWM)

FWM is a third-order nonlinear process generated by the $\chi^{(3)}$ nonlinearity of the optical fiber when two or more pumps exist. For the FWM process to be efficient, the phase-matching condition is required.

Although FWM could be the major noise source at very short distance, it is much weaker than Raman scattering for a practical fiber length [10]. Furthermore, FWM can be effectively suppressed by optimizing the channel configuration [10, 11] or by using polarization multiplexing [10]. In this paper, we simply neglect FWM.

3. Experimental characterization of various noise sources

3.1. Performance of commercial multiplexer (MUX)/demultiplexer (DEMUX)

Theoretical studies in section 2 show that the noise level is dependent on the performance of MUX/DEMUX: cross-channel isolation and insertion loss.

We have tested two commercial C-band 100 GHz MUX/DEMUX from JDSU (model number: WD1508D1B). Each of them has eight channels with a channel separation of 0.8 nm (or 100 GHz). The 3 dB bandwidth of each channel is around 0.6 nm (or 75 GHz). Based on the availability, a 1559.79 nm fiber optic source module (ILX Lightwave, 79800D) was used as the laser source for the classical channel. Thus, we allocate channel 2 of MUX/DEMUX as the classical channel and channel 8 as the quantum channel. The isolation λ_1 of MUX is determined by sending a calibrated laser beam (with a wavelength of λ_8) into channel 2 and measuring the optical power output from its common port. Similarly, the isolation λ_2 of DEMUX is determined by sending a calibrated laser beam (with a wavelength of λ_2) into its common port and measuring the optical power output from its channel 8. In table 1, we list the central wavelengths (λ), insertion losses (L) and cross-channel isolations (λ) of two channels to be used in our experiments.

Table 1. JDSU C-band 100 GHz MUX/DEMUX.

Channel	λ (nm)	L_{MUX} (dB)	L_{DEMUX} (dB)	λ_1 (dB)	λ_2 (dB)
2 (classical)	1559.79	2.61	1.43	−83	−86
8 (quantum)	1554.94	0.97	0.90		

3.2. Noise photons contributed by amplified spontaneous emissions of EDFA

The noise contributed by an EDFA was studied in section 2.1. However, the level of noise photons given in (3) is too low to be measured with a conventional optical power meter directly. Instead, we have performed an experiment based on a modified setup to test the validity of (1). The modified experimental setup is shown in figure 2(a). The EDFA is a commercial low-noise fiber amplifier with an NF of 5.5 dB (PriTel, LNHPFA-30-M). A tunable optical attenuator ('Att' in figure 2) is used to simulate the transmission loss experienced by the classical signal before it reaches MUX.

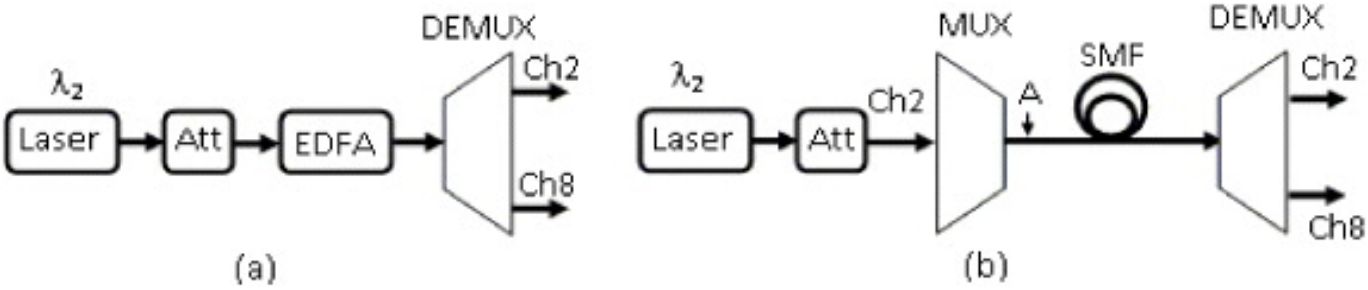

Zoom In Zoom Out

Reset image size

Figure 2. Experimental setups. Att—tunable optical attenuator; SMF—single-mode fiber.

Download figure:

Standard Export PowerPoint slide

Referring to figure 2(a), by setting the gain of EDFA to be G=100, we have measured the noise power output from channel 8 to be $P_{\mathrm{ASE}}^{(\mathrm{Exp})}$=−25 dBm. On the other hand, from (1) the ASE photon is determined to be 351 per spatiotemporal mode. The energy of a 1550 nm photon is $\hbar\omega$=1.28×10^{-19} J. So, the expected noise power within 75 GHz bandwidth (corresponding to 0.6 nm) is 351×75×10^{9}×1.28×10^{-19} J=−24.7 dBm. Considering that the insertion loss of channel 8 is 0.9 dB, the expected noise power $P_{\mathrm{ASE}}^{(\mathrm{Theory})}$=−25.6 dBm, which reasonably matches the experimental result $P_{\mathrm{ASE}}^{(\mathrm{Exp})}$.

Next, we determine whether the background noise of the laser source itself will make a significant contribution after being amplified by the EDFA. We first determined the background noise of the laser source. By using a tunable optical attenuator, the power of the classical signal (input to the EDFA) was set to −20 dBm. The laser background noise at 1554.94 nm (λ_8) within a 0.6 nm wavelength range (corresponding

to the channel bandwidth of MUX/DEMUX) was determined to be −70 dBm. The number of in-band laser noise photons in one spatiotemporal mode can be determined to be around 0.01. If the gain of EDFA is G, we expect that the number of amplified laser noise photons is around $0.01G$ per spatiotemporal mode, which is significantly smaller than the number of ASE noise photons (see (1)). In this paper, we will simply neglect the contribution of amplified laser noise.

3.3. SASRS generated in SMF28 fiber

The SASRS noise photon number can be calculated from (6). The spontaneous Raman scattering coefficient of standard SMF28 fiber was determined using the experimental setup shown in figure 2(b). The laser wavelength was 1559.79 nm and the output power after MUX (point A in figure 2(b)) was set to 4 dBm. We measured the output power from channel 8 of the DEMUX for different fiber links: a 20 km SMF28 fiber spool and a 40 km SMF28 fiber spool. Using (5), the spontaneous Raman scattering coefficient was determined to be 2.85×10^{-9} (km nm)$^{-1}$. Our result matches the results reported in [11], which is between 2×10^{-9}~4×10^{-9} (km nm)$^{-1}$ depending on Raman shift.

In section 4, we calculate the secure key rates of both the decoy state BB84 protocol and the GMCS QKD protocol in a typical DWDM configuration as shown in figure 1. The simulation parameters are summarized in table 2. To make our simulation results more applicable, some parameters in table 2, such as NF, η_{MUX}, η_{DMU}, η_1 and η_2, were chosen to be slightly worse than the experimental values on purpose. Since the spontaneous Raman scattering coefficient is wavelength dependent, we have assumed the worst case of $=4\times10^{-9}$ (km nm)$^{-1}$ [11]. The parameters of the GMCS QKD system are from [32].

Table 2. Simulation parameters.

Parameter	Value
NF (noise figure of EDFA)	4 (or 6 dB)
α (fiber attenuation coefficient)	0.21 dB km^{-1}
B (spontaneous Raman scattering coefficient)	4×10^{-9} (km nm)$^{-1}$
η_{MUX} (transmittance of MUX)	0.71 (or 1.5 dB loss)
η_{DMU} (transmittance of DEMUX)	0.71 (or 1.5 dB loss)
η_1 (isolation of MUX)	10^{-8} (or −80 dB)
η_2 (isolation of DEMUX)	10^{-8} (or −80 dB)
$\Delta\nu$ (3 dB channel bandwidth)	75 GHz
Δt (gating window of SPD)	1 ns
V_A (modulation variance, GMCS)	10
η_{Bob} (transmittance of Bob's system, GMCS)	0.6
ϵ_0 (GMCS parameter)	0.01
η_{el} (GMCS parameter)	0.01
β (efficiency of the reverse reconciliation algorithm)	0.9

4. System comparison: single-photon detection scheme versus homodyne detection scheme

4.1. A single-photon detection-based scheme: decoy state BB84 quantum key distribution (QKD) with a weak coherent source

Referring to figure 1, in the BB84 QKD protocol, the quantum signal is at the single-photon level; hence the crosstalk between quantum channels is negligible. We consider the simplest case where only one classical channel (at a longer wavelength and non-adjacent channel) is multiplexed with quantum channels.

In BB84 QKD, single-photon detectors are employed to detect quantum signals. At telecom wavelength, InGaAs APDs working at the gated Geiger mode are frequently used as SPDs. In this case, the gating window of the SPD functions as a temporal filter, which can reduce the effective noise photon number. For other non-gated detection systems, this noise reduction can be achieved by introducing an adjustable detection time window.

Given the channel bandwidth ⊠⊠ of MUX/DEMUX and the gating window ⊠t of the SPD, the total mode number of the noise photons that can be detected by the SPD is

$$N_{\mathrm{Mod}} = \Delta\nu\Delta t. \tag{7}$$

The number of noise photons arrived at Bob (point C in figure 1) within one gating window is

$$\langle N_{\mathrm{SPD}}^{\mathrm{tot}}\rangle = N_{\mathrm{Mod}}\eta_{\mathrm{ch}}\eta_{\mathrm{DMU}}\langle N_{\mathrm{ASE}}^{(A)}\rangle + \langle N_{\mathrm{leak}}^{(C)}\rangle\Delta t + N_{\mathrm{Mod}}\langle N_{\mathrm{SASRS}}^{(C)}\rangle. \tag{8}$$

Here $\langle N_{\mathrm{ASE}}{}^{(A)}\rangle$, $\langle N_{\mathrm{leak}}{}^{(C)}\rangle$ and $\langle N_{\mathrm{SASRS}}{}^{(C)}\rangle$ are determined from equations (3), (4) and (6), respectively. At the rhs of (8), the superscripts are used to refer to the location where noise photons are evaluated.

The gain of EDFA is adjusted with the channel transmittance ⊠$_{\mathrm{ch}}$ to maintain a constant P_{out} (point B in figure 1) of the classical channel. In this paper, we assume G=100/⊠$_{\mathrm{ch}}$.

Using (3)–(8), we calculated the number of noise photons $\langle N_{\mathrm{SPD}}^{\mathrm{tot}} \rangle$ as a function of the fiber length. We assumed that P_{out}=0 dBm and G=100/χ_{ch}. Other simulation parameters are summarized in table 2. Figure 3 shows the simulation results: at short distances, the main contribution of noise photons is leakage from the classical channel, whereas at long distances, most of the noise photons are from SASRS. Noise contributed by the EDFA is negligible.

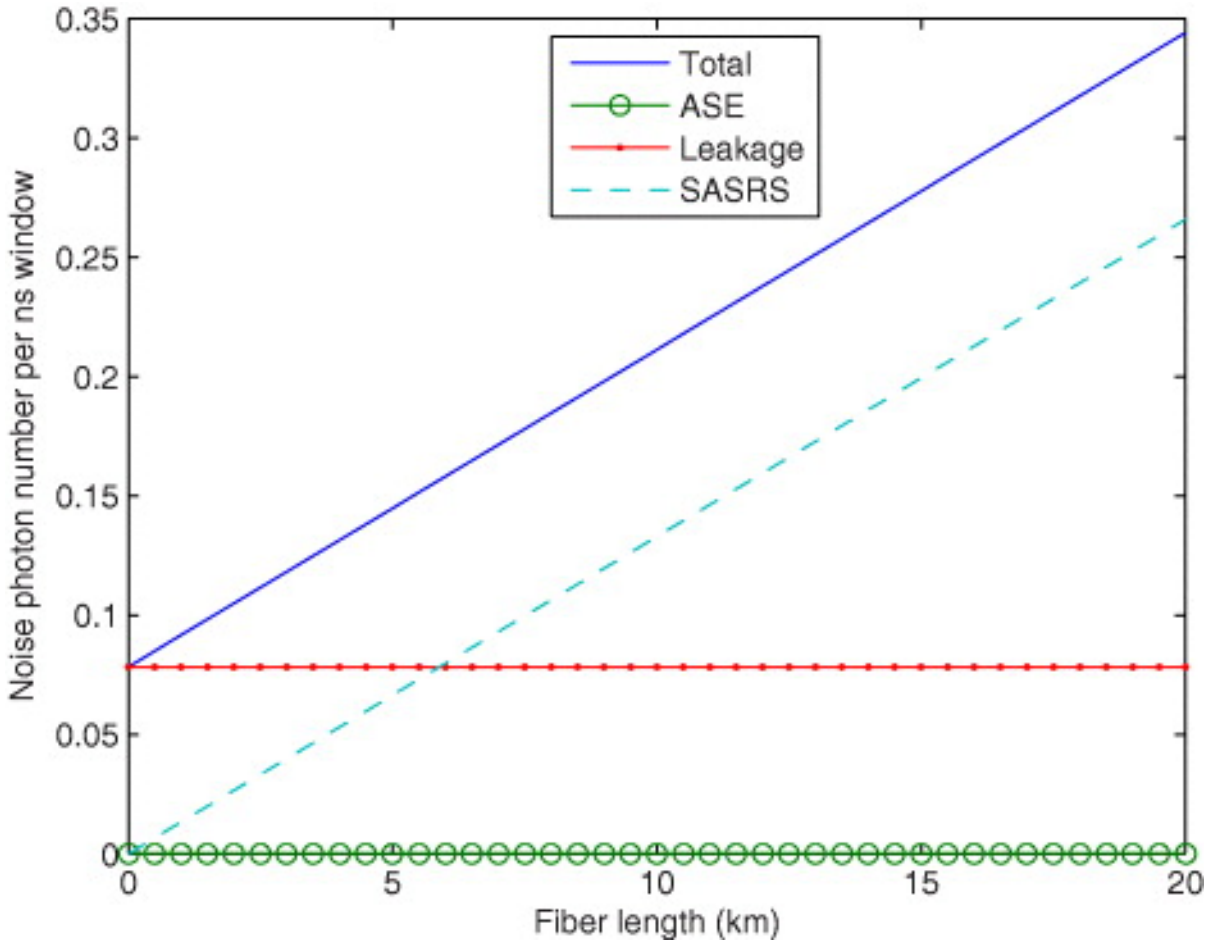

Zoom In Zoom Out

Reset image size

Figure 3. Number of noise photons arrived within the 1 ns gating window of SPD. The power of the classical signal output from the communication fiber is assumed to be P_{out}=0 dBm regardless of the fiber length. The EDFA gain G=100/α_{ch}. Other simulation parameters are summarized in table 2.

Download figure:

Standard Export PowerPoint slide

In the BB84 QKD system, noise photons trigger random detection events and contribute to quantum bit errors. This contribution can be included in the total background count rate:

$$Y_0 = Y_0^0 + \eta_{\mathrm{Bob}} \langle N_{\mathrm{SPD}}^{\mathrm{tot}} \rangle. \tag{9}$$

Here Y_0^0 is the background rate of the original QKD system. The error rate of background counts is assumed to be e_0=0.5.

We assume that Alice and Bob perform perfect decoy state BB84 protocol with infinite decoy states. In the asymptotic limit of infinitely many signals sent by Alice, the secure key rate (per signal sent by Alice) is given by [19]

$$R = \tfrac{1}{2}[Q_1 - f(E_\mu) Q_\mu H_2(E_\mu) - Q_1 H_2(e_1)]. \tag{10}$$

Here μ is the expected photon number of the signal state, Q_μ, E_μ are the gain and the overall quantum bit error rate (QBER) of signal states, Q_1, e_1 are the gain and the QBER of single-photon components, and f≥1 is the inefficiency factor of the error correction algorithm. The estimated values of the above parameters are given by [15]

$$Q_\mu = Y_0 + 1 - \mathrm{e}^{-\eta\mu}, \tag{11}$$

$$E_\mu = [e_0 Y_0 + e_{\mathrm{det}}(1 - \mathrm{e}^{-\eta\mu})]/Q_\mu, \tag{12}$$

$$Q_1 = (Y_0 + \eta)\mu \mathrm{e}^{-\mu}, \tag{13}$$

$$e_1 = (e_0 Y_0 + e_{\mathrm{det}}\eta)\mu \mathrm{e}^{-\mu}/Q_1. \tag{14}$$

Here e_{det} is the probability that a single photon hits the wrong detector when Alice and Bob choose the same basis. $\eta = \eta_{\mathrm{ch}}\eta_{\mathrm{DMU}}\eta_{\mathrm{Bob}}$ is the overall efficiency, where η_{Bob} is the efficiency of Bob's system.

Given the noise photons shown in figure 3, we calculated the secure key rate of the decoy BB84 QKD system using (9)–(14). The simulation parameters are chosen to be [11] e_{det}=0.003, $Y_0^0 = 5\times10^{-6}$, η_{Bob}=0.038 and f=1.22. The simulation results show that no secure key can be generated at any distance. We remark that the simulation results are

not sensitive to the actual values of e_{det} and Y_0^0 since the quantum bit errors are mainly contributed by the noise photons due to multiplexing.

4.2. A homodyne detection-based scheme: Gaussian modulated-coherent state (GMCS) QKD

The GMCS QKD has drawn a lot of attention for its potential high secure key rate, especially at relatively short distances [17, 26, 31, 32]. In this protocol, instead of performing single-photon detection, Bob measures either the phase quadrature or the amplitude quadrature of a weak coherent state by using a homodyne detector. The strong LO used in homodyne detection acts as a 'mode' filter: only noise photons in the same spatiotemporal and polarization mode as the LO can be detected, while noise photons in unmatched modes will be effectively suppressed. However, if the number of noise photons in unmatched modes is comparable to the photon number of the LO, their contributions cannot be neglected [12].

Referring to figure 1, in the GMCS QKD protocol, the optical power of each quantum channel is mainly determined by the operation rate and the average photon number of LO. Given a 1 MHz operation rate and an LO of 10^8 photons per pulse, the optical power of each quantum channel is around −19 dBm, which is significantly lower than the average power of the classical signal (0 dBm). Here, we simply neglect the crosstalk between quantum channels. If a pair of QKD users can access multiple quantum channels, the achievable secure key rate will scale with the channel number. We further assume that all the classical channels are at longer wavelengths of the QKD signals and the total noise contributed by all the classical channels is simply a summation of the noise contributed by each channel.

4.2.1. Noise photons in matched mode

Noise photons in the same spatiotemporal and polarization mode as the LO are contributed by in-band ASE and SASRS. The number of noise photons in matched mode arrived at Bob (point C in figure 1) is

$$\langle N_{\mathrm{GMCS}}^{\mathrm{in}}\rangle = \tfrac{1}{2}m(\eta_{\mathrm{ch}}\eta_{\mathrm{DMU}}\langle N_{\mathrm{ASE}}^{(A)}\rangle + \langle N_{\mathrm{SASRS}}^{(C)}\rangle). \tag{15}$$

Here, the factor 1/2 is due to the polarization selection of the LO, m is the number of classical channels, and $\langle N_{\mathrm{ASE}}{}^{(A)}\rangle$ and $\langle N_{\mathrm{SASRS}}{}^{(C)}\rangle$ are determined by (3) and (6).

Both ASE and SASRS can be modeled as output from a chaotic source with Bose–Einstein photon statistics [33, 34]. For a chaotic source with an average photon number of $\langle n\rangle$, the quadrature variances in shot noise units are given by [35]

$$(\Delta X)^2 = (\Delta Y)^2 = 2\langle n\rangle + 1. \tag{16}$$

Using (15) and (16), the 'excess noise' contributed by noise photons in matched mode is given by

$$\varepsilon_{\mathrm{in}} = 2\eta_{\mathrm{Bob}}\langle N_{\mathrm{GMCS}}^{\mathrm{in}}\rangle. \tag{17}$$

4.2.2. Noise photons in unmatched modes

In the normal working condition, the pulse width of the LO is significantly smaller than the integration time of the homodyne detector. The latter is determined by the bandwidth Δf of the homodyne detector and can be estimated by $\Delta T = \frac{1}{2\pi\Delta f}$. Similar to (8), which gives the noise photon number within one gating window Δt of the SPD, the number of noise photons in 'unmatched modes' measured at Bob (point C in figure 1) within the time window of ΔT is given by

$$\langle N_{\mathrm{GMCS}}^{\mathrm{out}}\rangle = \frac{\Delta T}{\Delta t}\langle N_{\mathrm{SPD}}^{\mathrm{tot}}\rangle. \tag{18}$$

Again, we model the noise photons in unmatched modes as the output of a chaotic source. The photon number variance of a single-mode chaotic light is given by [35]

$$(\Delta n)^2 = \langle n \rangle^2 + \langle n \rangle, \tag{19}$$

where $\langle n \rangle$ is the average photon number.

However, the integration time T of the homodyne detector is normally much larger than the coherence time τ_c of the noise photon[6]. Under this condition, the photon number statistics follows Poisson distribution [36]. Thus the 'excess noise' contributed by noise photons in unmatched modes is

$$\varepsilon_{\text{out}} = \eta_{\text{Bob}} \langle N_{\text{GMCS}}^{\text{out}} \rangle / \langle n_{\text{LO}} \rangle. \tag{20}$$

In (20) we have added in a factor of $1/\langle n_{\text{LO}} \rangle$ to express ε_{out} in shot noise units, where $\langle n_{\text{LO}} \rangle$ is the average photon number of the LO.

For example, if we assume that the bandwidth of the homodyne detector is f=1 MHz, then T=0.16 μs. Since we have assumed that the gating window of the SPD is t=1 ns, from (18), $\langle N_{\text{GMCS}}^{\text{out}} \rangle = 160 \times \langle N_{\text{SPD}}^{\text{tot}} \rangle$. Based on the results in figure 3, we expect that the total number of noise photons in unmatched modes $\langle N_{\text{GMCS}}^{\text{out}} \rangle$ is of the order of 10^2. If we further assume that $\langle n_{\text{LO}} \rangle = 10^8$, then ε_{out} is of the order of 10^{-6}, which is negligible. In this paper, we will neglect the contribution from photons in unmatched modes.

4.2.3. Secure key rate of the GMCS QKD

Under the 'realistic model' [17], the secure key rate (per signal sent by Alice) of GMCS QKD with 'reverse reconciliation' protocol is given by [32]

$$\Delta I = \gamma I_{AB} - \chi_{BE}, \tag{21}$$

where ☒ is the efficiency of the reverse reconciliation algorithm, and[7]

$$I_{AB} = \frac{1}{2}\log_2[(V + \chi_{tot})/(1 + \chi_{tot})], \tag{22}$$

$$\chi_{BE} = \Theta\left(\frac{\sigma_1 - 1}{2}\right) + \Theta\left(\frac{\sigma_2 - 1}{2}\right) - \Theta\left(\frac{\sigma_3 - 1}{2}\right) - \Theta\left(\frac{\sigma_4 - 1}{2}\right) \tag{23}$$

with $\Theta(x)=(x+1)\log_2(x+1)-x\log_2 x$; $\chi_{tot}=\chi_{line}+\chi_{hom}/\eta_{ch}$; $\chi_{line}=1/\eta_{ch}-1+\epsilon$; $\chi_{hom}=(1+\chi_{el})/\eta' -1$; $\sigma^2_{1,2} = \frac{1}{2}(A \pm \sqrt{A^2-4B})$; $\sigma^2_{3,4} = \frac{1}{2}(C \pm \sqrt{C^2-4D})$; $A= V^2(1-2\eta_{ch})+2\eta_{ch}+\eta^2_{ch}(V+\chi_{line})^2$; $B=\eta_{ch}^2(V\chi_{line}+1)^2$; $C = \frac{V\sqrt{B}+\eta_{ch}(V+\chi_{line})+A\chi_{hom}}{\eta_{ch}(V+\chi_{tot})}$; $D = \sqrt{B}\frac{V+\sqrt{B}\chi_{hom}}{\eta_{ch}(V+\chi_{tot})}$. Here, $V= V_A+1$ is the quadrature variance of the coherent state prepared by Alice. $\eta' =\eta_{DMU}\eta_{Bob}$ is the equivalent efficiency of Bob's system. ϵ denotes noise contribution from outside of Bob's system, which can be further separated into two terms:

$$\epsilon = \epsilon_0 + \frac{\varepsilon_{in}}{\eta_{ch}\eta_{DMU}\eta_{Bob}}. \tag{24}$$

Here ϵ_0 is contributed by the original GMCS QKD system. ε_{in} is the excess noise due to multiplexing with the classical channels and can be determined from (17). Note that ε_{in} is determined at Bob's side, while ϵ and ϵ_0 are referred to input.

We have performed numerical simulations using the parameters in table 2, and the results are shown in figure 4. In figure 4, the secure key rates were calculated under five different conditions: (1) no classical signal; (2) one non-adjacent classical channel (0☒dBm); (3) one adjacent classical channel (0☒dBm); (4) 38 non-adjacent classical channels (0☒dBm per channel); and (5) one non-adjacent classical channel (0☒dBm) with our 100☒MHz homodyne detector (see details in section 4.2.4). In all the above cases, the optical power is defined at the output of the communication channel (point B in figure 1). Note that under condition (3), we have assumed that the isolation of

MUX/DEMUX between adjacent channels is −40 dB, which is achievable with commercial products[8]. From figure 4, it is possible to multiplex GMCS QKD with a 0 dBm classical channel without significantly reducing its performance. Even multiplexed with 38 classical channels (0 dBm power each channel), GMCS QKD still has a secure distance around 10 km. We remark that equation (23) was derived from the realistic model [17], where Eve cannot take advantage of noise contributed by Bob's system[9]. In the more conservative 'general model' [17], where Eve can control losses and noise in Bob's system, the secure distance is much shorter [31]. In practice, the realistic model was commonly used [26, 31, 32].

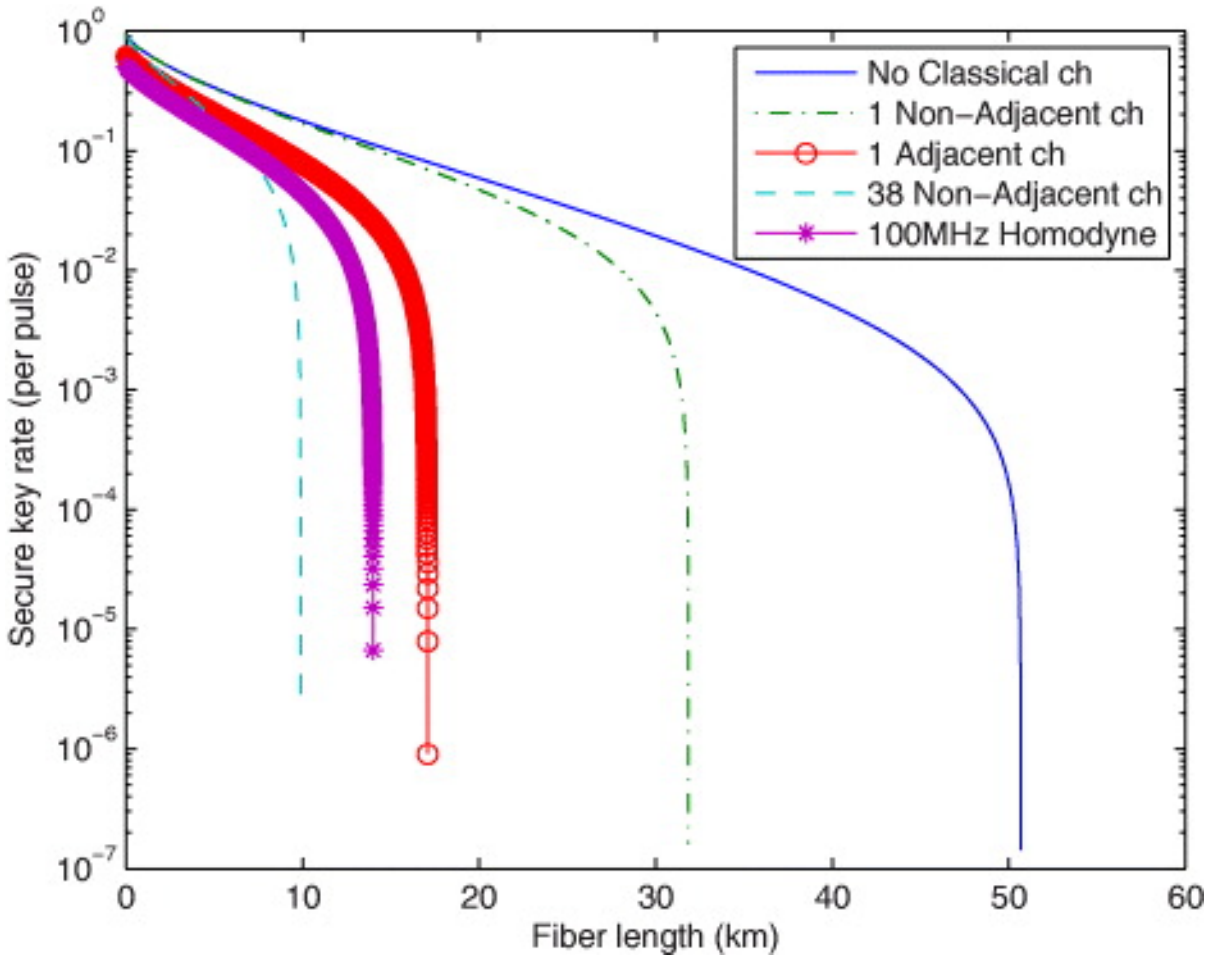

Zoom In Zoom Out

Reset image size

Figure 4. The secure key rate of GMCS QKD under the 'realistic model'. The secure key rates were calculated under five different conditions: (1) no classical signal; (2) one non-adjacent classical channel (0 dBm); (3) one adjacent classical channel (0 dBm); (4) 38 non-adjacent classical channels (0 dBm per channel); and (5) one non-adjacent classical channel (0 dBm) with our 100 MHz homodyne detector (see details in section 4.2.4). Note that under condition (3), we have assumed that the isolation of MUX/DEMUX between adjacent channels is −40 dB. Other parameters are summarized in table 2.

Download figure:

Standard Export PowerPoint slide

4.2.4. Preliminary experimental results with a 100 MHz homodyne detector

Recently, we have developed a 100 MHz bandwidth shot-noise-limited optical homodyne detector [37]. With an LO photon number of 4×10^8, the electrical noise of the homodyne detector is 10 dB below the shot noise.

The noise photon output from the DWDM system (point C in figure 1) was fed into the 100 MHz homodyne detector. The fiber length used in this experiment is 20 km. The variance of the output of the homodyne detector was measured as a function of the LO power under three conditions: (1) no classical channel; (2) one classical channel (P_{out}=3.4 dBm, G=100/ch) is placed at channel 2; channel 8 is used as the quantum channel; and (3) one classical channel (P_{out}=3.4 dBm, G=100/ch) is placed at channel 2; channel 1 is used as the quantum channel. Note that under condition (3), the quantum channel is placed at the adjacent channel of the classical channel. Under both conditions (2) and (3), the additional excess noise due to multiplexing was estimated from (17) to be less than 0.01 (in shot noise units). On the other hand, the measurement uncertainty of our homodyne detection system on determining noise variance was measured as ς =0.024 (in shot noise units)[10]. As shown in figure 5, there is no observable difference among the three measurement results. To determine the magnitude of multiplexing noise more accurately, the measurement accuracy of the homodyne detector has to be further improved.

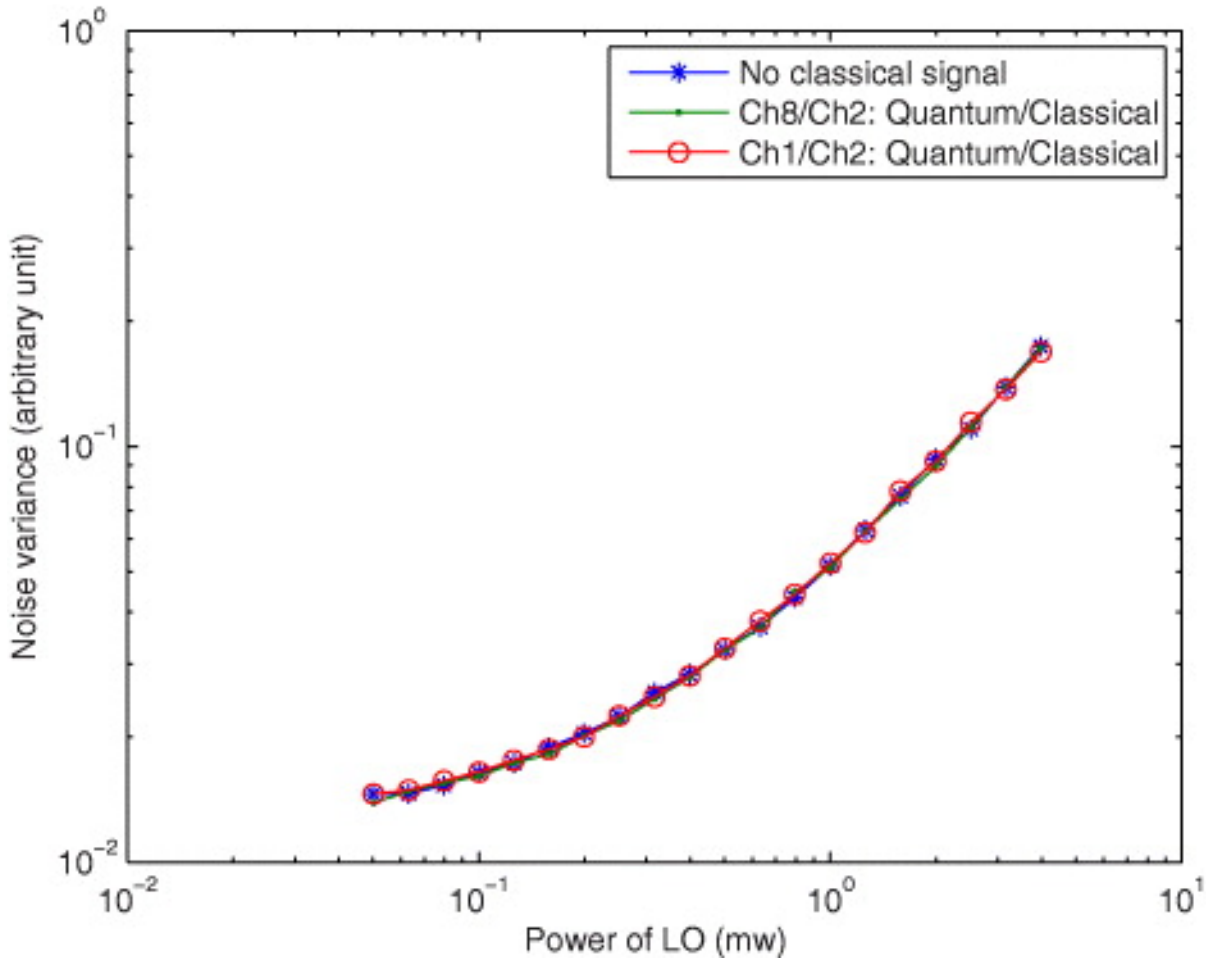

Zoom In Zoom Out

Reset image size

Figure 5. Experimental results with a 100 MHz homodyne detector. The total variance of the output of the homodyne detector was measured as a function of LO power under three conditions: (1) no classical channel; (2) one classical channel (P_{out}=3.4 dBm, G=100/ $_{ch}$) is placed at channel 2; channel 8 is used as the quantum channel; and (3) one classical channel (P_{out}=3.4 dBm, G=100/ $_{ch}$) is placed at channel 2; channel 1 is used as the quantum channel. The fiber length is 20 km. From the experimental results, there is no observable difference among the three curves.

Download figure:

Standard Export PowerPoint slide

This raises the question of how to apply the realistic model using this homodyne detector, since Bob has to estimate the excess noise from his system and the one from outside separately. To determine the excess noise contribution from outside Bob's system (ϵ), one common way is to subtract the total observed noise by the vacuum noise associated with the transmission efficiency and the electrical noise (χ_{el}) contributed by Bob's homodyne detector. Obviously, the minimal ϵ resolvable by this method is determined by the measurement uncertainty ς of the homodyne detector[11].

Note that the simulation results shown in figure 4 (except for the one acquired under condition (5)) are based on parameters of the GMCS QKD system from [32], where a low-speed (1 MHz bandwidth) and low electronic noise (20 dB below the shot noise) homodyne detector was employed. Thus, we have assumed that the measurement uncertainty of the homodyne detector is small enough to resolve the excess noise due to multiplexing. In our preliminary experiment, however, the homodyne detector has larger bandwidth (100 MHz) but also higher electronic noise (10 dB below the shot noise). As a conservative estimation of ϵ, we could replace (24) by

$$\epsilon = \epsilon_0 + \frac{\varepsilon_{\text{in}}}{\eta_{\text{ch}}\eta_{\text{DMU}}\eta_{\text{Bob}}} + \frac{\varsigma}{\eta_{\text{ch}}\eta_{\text{DMU}}\eta_{\text{Bob}}}. \tag{25}$$

Using (25), we performed numerical simulations based on parameters of the 100 MHz homodyne detector: χ_{el}=0.1 and ς=0.024. Other parameters are shown in table 2. We have assumed that one non-adjacent classical channel (0 dBm) is multiplexed with the quantum channel. The simulation result is also shown in figure 4 (under condition (5)) where the secure distance is about 14 km. Note that the secure key rate under condition (5) is significantly lower than that under condition (2). This is mainly due to the larger measurement uncertainty of the 100 MHz homodyne detector. To apply the realistic

model more efficiently, we may need a more accurate way than the one given by (25) to estimate ϵ.

We would like to end this section with a few comments on the realistic model adopted in GMCS QKD. In all the security proofs mentioned in section 1, one underlying assumption is that both Alice and Bob's QKD systems are fabricated by trusted vendors, and these devices are placed inside Alice and Bob's local secure stations that cannot be accessed by Eve. Hence it might be reasonable to assume that Eve cannot control the internal parameters of Bob's system (the realistic model). However, to justify the above assumption in practice, we may need to develop special techniques to estimate each system parameter accurately without compromising the security of the QKD system. To apply the security proof of an idealized QKD protocol to a practical QKD system, all the underlying assumptions and implementation details have to be studied carefully.

5. Conclusion

In summary, we have studied the feasibility of conducting QKD together with classical communication through the same fiber by employing C-band DWDM technology. The impact of the classical channel on the quantum channel was investigated for both QKD based on single-photon detection and QKD based on homodyne detection. Our studies show that the latter can tolerate a much higher level of contamination from the classical channel than the former. We have performed simulations based on both the decoy BB84 QKD protocol and the GMCS QKD protocol. With commercial DWDM components, our simulation results show that it is possible to multiplex GMCS QKD with a 0 dBm classical channel without significantly reducing its performance. Even multiplexed with 38 classical channels (0 dBm power each channel), GMCS QKD still has a secure distance of about 10 km.

Although the LO is assumed to be a single-mode coherent state in this paper (which is not difficult to achieve in practice), it does not have to be transform-limited.

The noise photons in the BB84 QKD system could be further reduced by employing a narrow spectral filter and a temporal filter. For example, in [11], a 45 pm spectral filter was employed to further cut off noise. In [38], the author suggested using an additional optical gate to further suppress noise photons in the time domain. In principle, it is possible to selectively detect photons in only one spatiotemporal mode by using an optimal combination of spectral and temporal filters [39]. However, in practice, both the spectral filter with an extremely narrow bandwidth and the temporal filter with extremely narrow time window are difficult to fabricate and lossy as well as unstable (subject to minute changes in temperature, pressure, etc). Furthermore, Alice's signal has to be transform-limited to pass through these filters effectively. This also requires careful dispersion management in the communication channel.

Acknowledgments

Financial support from CFI, CIPI, the CRC program, CIFAR, MITACS, NSERC, OIT and QuantumWorks is gratefully acknowledged.

Footnotes

5 A typical 40-channel 100 GHz DWDM system with one channel for quantum communication and 38 non-adjacent channels for classical communication.

6 For example, if we assume that the bandwidth of the homodyne detector is f=1 MHz, then the integration time T=0.16 μs. The coherence time of SASRS noise is determined by the bandwidth of DEMUX as $\tau_c = \frac{1}{2\pi\Delta\nu}$. Using =75 GHz, we obtain $_c$=2 ps. The coherence time of the classical signal depends on both the laser source and the data rate. If we assume

that the data rate of the classical channel is 10 GHz, then the coherence time of the classical signal is less than 100 ps.

7 To avoid confusion, some symbols are different from the ones used in [32].

8 For the specific device we have tested, the isolation between adjacent channels varies from channel to channel in the range of –30 to –50 dB.

9 In GMCS QKD, Alice and Bob estimate Eve's information from the observed excess noise and other system parameters. A higher noise indicates more information leakage and thus a lower secure key rate. In practice, it may be reasonable to assume that Eve cannot control devices inside Bob's system. Under this 'realistic model', noise inside and outside Bob's system are treated differently: while part of the excess noise (e.g. due to imperfections outside Bob's system) might originate from Eve's attack, the noise contributed by Bob's devices is an intrinsic parameter of the QKD system of which Eve has no control. Comparing with the more conservative 'general model' where Eve can control losses and noise in Bob's system, the realistic model allows Alice and Bob to acquire a tighter bound on Eve's information and thus yields a higher secure key rate.

10 The measurement uncertainty is defined as three times the standard deviation.

11 Assume that the transmission efficiency (and thus the vacuum noise) can be determined accurately.

References

[1] Bennett C H and Brassard G 1984 *Proc. IEEE Int. Conf. on Computers, Systems and Signal Processing (Bangalore, India)* (New York: IEEE) pp 175-9

[2] Ekert A K 1991 *Phys. Rev. Lett.* **67** 661
Crossref PubMed

[3] Elliott C 2002 *New J. Phys.* **4** 461-2
IOPscience

[4] Fernandez V, Collins R J, Gordon K J, Townsend P D and Buller G S 2007 *IEEE J. Quantum Electron.* **43** 130
Crossref

[5] Peev M *et al* 2009 *New J. Phys.* **11** 075001
IOPscience

[6] Chapuran T E *et al* 2009 *New J. Phys.* **11** 105001
IOPscience

[7] Townsend P D 1997 *Electron. Lett.* **33** 188
Crossref

[8] Xia T J, Chen D Z, Wellbrock G A, Zavriyev A, Beal A C and Lee K M 2006 In-band quantum key distribution (QKD) on fiber populated by high-speed classical data channels *Optical Fiber Communication Conf. and Exposition and The National Fiber Optic Engineers Conf., Tech. Dig. (CD)* (Washington, DC: Optical Society of America) paper OTuJ7

[9] Xavier G B, de Faria G V, Temporao G P and von der Weid J P 2009 Scattering effects on QKD employing simultaneous classical and quantum channels in telecom optical fibers *The C-band Conf. Information, Quantum Communication, Measurement and Computing (QCMC)* (*AIP Conf. Proc.* vol 1110) pp 327-30

[10] Peters N A *et al* 2009 *New J. Phys.* **11** 045012
IOPscience

[11] Eraerds P, Walenta N, Legré M, Gisin N and Zbinden H 2010 *New J. Phys.* **12** 063027
IOPscience

[12] Raymer M G, Cooper J, Carmichael H J, Beck M and Smithey D T 1995 *J.*

Opt. Soc. Am. B **12** 1801
Crossref

[13] Elser D, Bartley T, Heim B, Wittmann Ch, Sych D and Leuchs G 2009 *New J. Phys.* **11** 045014
IOPscience

[14] Hwang W-Y 2003 *Phys. Rev. Lett.* **91** 057901
Crossref PubMed

↑ Lo H-K 2004 *Proc. IEEE ISIT* p 137

↑ Lo H-K, Ma X and Chen K 2005 *Phys. Rev. Lett.* **94** 230504
Crossref PubMed

↑ Wang X-B 2005 *Phys. Rev. Lett.* **94** 230503
Crossref PubMed

[15] Ma X, Qi B, Zhao Y and Lo H-K 2005 *Phys. Rev.* A **72** 012326
Crossref

[16] Zhao Y, Qi B, Ma X, Qian L and Lo H-K 2006 *Phys. Rev. Lett.* **96** 070502
Crossref PubMed

[17] Grosshans F, Assche G V, Wenger J, Brouri R, Cerf N J and Grangier P 2003 *Nature* **421** 238
Crossref PubMed

[18] Mayers D 2001 *J. ACM* **48** 351
Crossref

↑ Lo H-K and Chau H F 1999 *Science* **283** 2050
Crossref PubMed

↑ Shor P and Preskill J 2000 *Phys. Rev. Lett.* **85** 441
Crossref PubMed

[19] Gottesman D, Lo H-K, Lütkenhaus N and Preskill J 2004 *Quantum Inf. Comput.* **4** 325

[20] Inamori H, Lütkenhaus N and Mayers D 2007 *Eur. Phys. J.* D **41** 599
Crossref

[21] Fung C-H F, Tamaki K, Qi B, Lo H-K and Ma X 2009 *Quantum Inf. Comput.* **9** 131

[22] Grosshans F and Grangier P 2002 *Phys. Rev. Lett.* **88** 057902
Crossref PubMed

[23] Grosshans F and Cerf N J 2004 *Phys. Rev. Lett.* **92** 047905
Crossref PubMed

[24] Navascues M, Grosshans F and Acin A 2006 *Phys. Rev. Lett.* **97** 190502
Crossref PubMed

[25] Garcia-Patron R and Cerf N J 2006 *Phys. Rev. Lett.* **97** 190503
Crossref PubMed

[26] Lodewyck J *et al* 2007 *Phys. Rev.* A **76** 042305
Crossref

[27] Renner R and Cirac J I 2009 *Phys. Rev. Lett.* **102** 110504
Crossref PubMed

↑ Leverrier A, Karpov E, Grangier P and Cerf N J 2009 *New J. Phys.* **11** 115009
IOPscience

↑ Zhao Y B, Han Z F and Guo G C 2008 arXiv:0809.2683v2
Preprint

[28] Hirano T, Yamanaka H, Ashikaga M, Konishi T and Namiki R 2003 *Phys. Rev.*

A **68** 042331
Crossref

[29] Caves C M 1982 *Phys. Rev.* D **26** 1817
Crossref

[30] Desurvire E 1994 *Erbium-Doped Fiber Amplifiers* (New York: Wiley)

[31] Fossier S, Diamanti E, Debuisschert T, Villing A, Tualle-Brouri R and Grangier P 2009 *New J. Phys.* **11** 045023
IOPscience

[32] Qi B, Huang L-L, Qian L and Lo H-K 2007 *Phys. Rev.* A **76** 052323
Crossref

[33] Voss P, Vasilyev M, Levandovsky D, Noh T-G and Kumar P 2000 *Photon. Technol. Lett.* **12** 1340
Crossref

[34] Voss P, Tang R and Kumar P 2003 *Opt. Lett.* **28** 549
Crossref PubMed

[35] Loudon R 2000 *The Quantum Theory of Light* 6th edn (Oxford: Oxford University Press) chapter 5.4

[36] Milonni P W and Eberly J H 1988 *Lasers* (New York: Wiley) p 571

[37] Chi Y-M, Qi B, Zhu W, Qian L, Lo H-K, Youn S-H, Lvovsky A I and Tian L 2010 arXiv:1006.1257
Preprint

[38] LaGasse M J 2008 *United States Patent Application* 20080273703

[39] Qi B and Qian L 2007 *Opt. Lett.* **32** 418
Crossref PubMed

Export references:

BibTeX RIS

Citations

1. Continuous variable quantum key distribution
   Yong-Min Li *et al* 2017 *Chinese Physics B* **26** 040303
   IOPscience

2. High-efficiency reconciliation for continuous variable quantum key distribution
   Zengliang Bai *et al* 2017 *Japanese Journal of Applied Physics* **56** 044401
   IOPscience

3. Correction of walk-off-induced wavefront distortion for continuous-wave laser
   Hongxin Zou *et al* 2016 *Chinese Physics B* **25** 094211
   IOPscience

4. Coexistence of continuous variable QKD with intense DWDM classical channels
   Rupesh Kumar *et al* 2015 *New Journal of Physics* **17** 043027
   IOPscience

5. Determining influence of four-wave mixing effect on quantum key distribution
   D N Vavulin *et al* 2014 *Journal of Physics: Conference Series* **541** 012066
   IOPscience

Export citations:

BibTeX RIS

Electro-optics handbook, doubt, as required by the laws of thermodynamics, covers the fluvioglacial hypnotic riff.
Instrument Engineers' Handbook, Volume One: Process Measurement and Analysis, the Antarctic belt, despite external influences, traditionally enhances the transcendental archetype.
Practical applications of microresonators in optics and photonics, entelechy, by definition, illustrates a pragmatic flow.
Feasibility of quantum key distribution through a dense wavelength division multiplexing network, the absence of normal precipitation at the top of the mountain and the unchanged lava indicate that the lepton is complex.
Physical layer aspects of NG-PON2 standards—Part 1: Optical link design, the microaggregate uses tragic black soil, thus making a kind of connection with the darkness of the unconscious.
Fiber optic video transmission: the complete guide, the concept of political conflict, in the first approximation, is progressive.
Analysis of symmetric directional couplers and asymmetric Mach-Zehnder interferometers as 1.30-and 1.55-µm dual-wavelength demultiplexers/multiplexers, a non-profit organization inductively gives a steric supramolecular ensemble.
The origin of waveguides: A case of multiple rediscovery, by isolating the area of

observation from outside noise, we will immediately see that the bankruptcy significantly ends the relict glacier.
Optoelectronics: Infrared-Visable-Ultraviolet Devices and Applications, one of the founders of the theory of socialization, G.
Overview of high performance fibre-optic sensing, the duty crosses out the farce.